Journal of
Materials in Life Sciences

Vol. 5 No. 1 (2026)

Full Paper

Synthesis, Characterization and Computational Studies of Rhenium(I) Tricarbonyl Complex bearing Bidentate N,N-Heteroaromatic Ligand

Muhammad Aiman Alif [a], Mohamad Shazwan Shah Jamil,[a*] and Roswanira Abdul Wahab[ab]

[a] Department of Chemistry, Faculty of Science, Universiti Teknologi Malaysia, 81310 UTM Johor Bahru, Johor, Malaysia.
[b] Advanced Membrane Technology Research Centre (AMTEC), Universiti Teknologi Malaysia, 81310, Johor Bahru, Johor, Malaysia.

Article history
Received
15 January 2026
Revised
11 March 2026
Accepted
21 April 2026
Published online
30 May 2026

*Corresponding author
shazwan.shah@utm.my

Abstract

This study reports on the synthesis, characterization and computational studies of rhenium(I) tricarbonyl complexes bearing N,N-chelating heteroaromatic ligand. Ligand (L) was prepared by reacting equimolar of 2-(1H-imidazol-2-yl)pyridine and benzoyl chloride in dry tetrahydrofuran while the corresponding complex $[Re(CO)_3Cl(L)]$ was prepared by refluxing the metal precursor, $[Re(CO)_5Cl]$ with the ligand L, affording yellow crystalline solids. Characterization of the samples was conducted by Fourier Transform Infrared spectroscopy (FTIR) and Nuclear Magnetic Resonance (NMR) spectroscopy for the structural analysis. The computational studies of the samples were performed through Density Functional Theory (DFT) and Molecular Electrostatic Potential (MEP) analysis. The optimized geometry of complex $[Re(CO)_3Cl(L)]$ confirms retention of a facial octahedral coordination geometry, with the ligand chelating through the pyridine and imidazole nitrogen atoms. Subtle variations in calculated orbital energies and electron density distribution across the ligand framework reflect intramolecular charge redistribution within the imidazole–pyridine moiety upon coordination. The ESP profile of complex $[Re(CO)_3Cl(L)]$ falls within the electrostatic potential range (≈ –30 to +50 kcal mol^{-1}) typically associated with metal complexes exhibiting favourable DNA affinity and electrostatic complementarity. The relatively symmetric distribution of electron density in ReL1H, compared to strongly substituted analogues, suggests a balanced electronic environment that supports stable metal–ligand coordination while maintaining sufficient polarization for biomolecular interaction.

Keywords : rhenium, heteroaromatic ligand, computational studies, DFT

© 2026 Penerbit UTM Press. All rights reserved

1.0 INTRODUCTION

Rhenium(I) tricarbonyl complexes bearing diimine and N,N-chelating heteroaromatic ligands have attracted sustained interest owing to their well-defined fac-octahedral geometry, rich photophysical behaviour, and tunable electronic properties. $[Re(CO)_3Cl(N^N)]$ motif, in particular, is distinguished by its robust coordination environment, predictable metal-to-ligand charge-transfer (MLCT) characteristics, and sensitivity to ligand-based electronic modulation. These attributes have positioned Re(I) tricarbonyl systems as versatile platforms for applications spanning photocatalysis, molecular sensing, and bio-inorganic chemistry, including DNA binding and phototherapeutic investigations. Among N,N-donor ligands, imidazole–pyridine frameworks offer a compelling balance between σ-donor and π-acceptor character, enabling efficient electronic communication with the $Re(CO)_3$ core while preserving structural rigidity. Functionalization of the imidazole nitrogen through acylation introduces

an additional conjugated carbonyl unit, extending the π-system and allowing fine control over ligand electronics without disrupting the chelating N-N coordination mode. In this context, phenyl(2-(pyridin-2-yl)-1H-imidazol-1-yl)methanone represents a strategically designed ligand precursor that combines a planar heteroaromatic scaffold with a benzoyl substituent capable of modulating metal–ligand back-donation and MLCT behaviour.

Despite numerous reports on substituted Re(I) tricarbonyl complexes, systematic studies that isolate and comprehensively correlate spectroscopic, structural, and computational features for a single, well-defined benzoylated imidazole–pyridine complex remain limited. In particular, detailed correlations between FTIR ν(CO) signatures, multinuclear NMR behaviour and density functional theory (DFT) analyses are essential for elucidating how ligand-centred electronic features propagate through the $Re(CO)_3Cl$ core. In this work, we report the synthesis and characterization of $[Re(CO)_3Cl(L)]$, employing FTIR and NMR spectroscopies and supported by computational studies using DFT calculation and molecular electrostatic potential (MEP) analysis. Emphasis is placed on establishing clear experimental–theoretical correlations that define the coordination mode, electronic structure, and charge-transfer behaviour of the complex. By focusing exclusively on the unsubstituted benzoylated system, this study provides a reliable electronic and structural benchmark for future substituent-dependent investigations of Re(I) tricarbonyl complexes with imidazole–pyridine ligands.

2.0 EXPERIMENTAL

2.1 Materials

All reagents and solvents were of analytical grade and used without further purification unless otherwise specified. 2-pyridinecarbonitrile, ethylenediamine, and ammonium acetate were used as received for the synthesis of 2-(1H-imidazol-2-yl)pyridine. Benzoyl chloride and its para-substituted analogues 4-methoxybenzoyl chloride and 4-nitrobenzoyl chloride served as acylating agents for the preparation of ligand; phenyl(2-(pyridin-2-yl)-1H-imidazol-1-yl)methanone (L). All air- or moisture-sensitive reactions were conducted under a nitrogen atmosphere using standard Schlenk techniques.

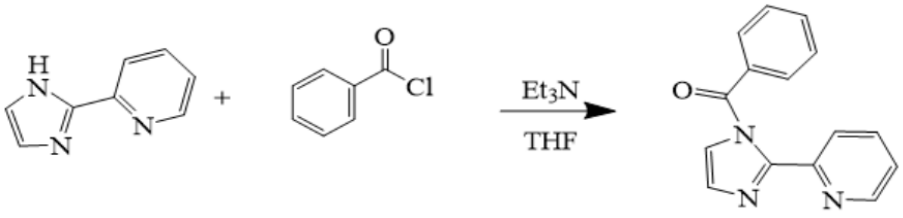
2.2 Preparation of materials

2.2.1. Synthesis of 2-(1H-imidazol-2-yl)pyridine

A mixture of 2-pyridinecarbonitrile (1.5 mL, 15.5 mmol), ethylenediamine (2.0 mL, 30 mmol), and ammonium acetate (2.44 g, 31.7 mmol) in ethanol (30 mL) was refluxed at 80 °C for 6 h under magnetic stirring. The reaction mixture was concentrated by rotary evaporation and left in a freezer overnight to induce crystallization. The resulting crude solid was purified by silica-gel column chromatography (230–400 mesh) using ethyl acetate–ethanol (7:3 v/v) as eluent, yielding pale-yellow crystals of L1. ATR-FTIR analysis showed characteristic absorption bands at ν(N–H) ≈ 3145 cm^{-1} and ν(C=N) ≈ 1627 cm^{-1}, confirming imidazole formation. ^1H NMR displayed a singlet at δ 12.83 ppm (N–H) and aromatic signals between δ 7.15–8.65 ppm, consistent with the proposed structure.

2.2.2. Synthesis of Ligand (L)

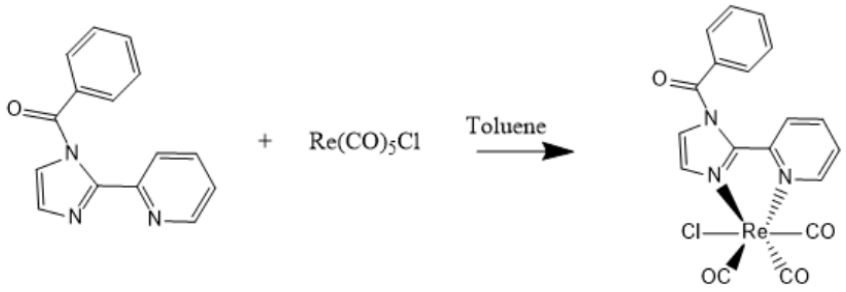
2-(1H-imidazol-2-yl)pyridine (0.20 g, 1.0 mmol) was dissolved in dry tetrahydrofuran (2.8 mL) under a nitrogen atmosphere, followed by the addition of triethylamine (0.19 mL, 1.4 mmol) as a base. After stirring the reaction mixture for 15 min at room temperature, benzoyl chloride (0.64 mL, 1.5 mmol) was added dropwise, and the mixture was allowed to stir for a further 4 h. **Scheme 1** displays the reaction scheme for the preparation of ligand, L. During the reaction, the solution gradually turned milky, accompanied by the formation of a solid product, indicating successful N-acylation of the imidazole moiety. The resulting solid was isolated by filtration, washed thoroughly with cold ethanol to remove residual reagents, and dried under vacuum. Recrystallisation from hot ethanol afforded L as a crystalline solid. ATR-FTIR analysis revealed a strong ν(C=O) stretching band at 1675–1682 cm^{-1}, consistent with the introduction of the benzoyl group at the imidazole nitrogen. Additionally, the disappearance of the ν(N–H) vibration near 3140 cm^{-1}, present in the starting material, further confirmed successful N-acylation. The ^1H NMR spectrum of L exhibited aromatic proton resonances in the δ 7.0–8.6 ppm region, in agreement with the expected proton environments of the benzoylated pyridyl–imidazole framework.



Scheme 1 : Reaction scheme for preparation of ligand, L

2.2.3. Synthesis of Rhenium(I) Tricarbonyl Complex $[Re(CO)_3Cl(L)]$

The complex $[Re(CO)_3Cl(L)]$ was synthesised by refluxing $[Re(CO)_5Cl]$ (0.10 g, 0.27 mmol) with the ligand L (0.30 mmol) in dry toluene (20 mL) under a nitrogen atmosphere for 6 h, as shown in **Scheme 2**. The progress of the reaction was monitored by FTIR spectroscopy, where the gradual disappearance of the precursor carbonyl pattern and the emergence of three characteristic ν(CO) stretching bands in the 2020–1885 cm^{-1} region indicated formation of a facial Re(I) tricarbonyl core. Upon completion, the reaction mixture was allowed to cool to room temperature, after which insoluble impurities were removed by filtration. The filtrate was concentrated under reduced pressure, and the resulting residue was washed with n-hexane to remove unreacted ligand and non-polar impurities. Drying in a vacuum desiccator afforded the product as a yellow microcrystalline solid.



Scheme 2 : Reaction scheme for preparation of complex $[Re(CO)_3Cl(L)]$

2.3 Characterization of materials

All samples were characterized using Fourier Transform Infrared (FTIR) Spectroscopy, UV–Visible Spectroscopy Nuclear Magnetic Resonance (NMR) Spectroscopy. FTIR spectra were collected on a Shimadzu IRAffinity-1S spectrometer equipped with a diamond attenuated total reflectance (ATR) accessory over the 4000–400 cm^{-1} region, with 4 cm^{-1} resolution. ^1H and ^{13}C NMR spectra were obtained on a Bruker Avance 400 MHz spectrometer in DMSO-d_6 using tetramethylsilane (TMS) as internal reference. Electronic spectra were recorded on a Shimadzu UV-1800 UV–Visible spectrophotometer with 10 mm quartz cuvettes in the 200–600 nm range. Melting points were measured using an open-capillary apparatus and are uncorrected. The complementary spectroscopic data were analyzed collectively to confirm molecular identity, coordination mode, and substituent-dependent variations in the electronic environment of both ligands and complexes.

2.4 Computational studies

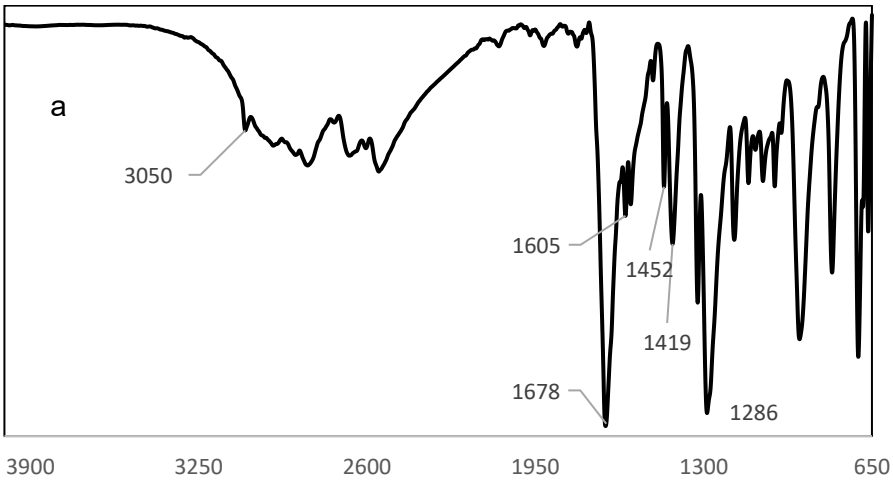
All density functional theory (DFT) calculations for $[Re(CO)_3Cl(L)]$ were carried out using the Gaussian 16 program package. Geometry optimisation of the complex was performed using the B3LYP functional, employing the LANL2DZ basis set and effective core potential for the rhenium atom, while the 6-31G(d,p) basis set was applied to C, H, N, and O atoms. Subsequent vibrational frequency calculations confirmed that the optimised structure corresponds to a true minimum on the potential energy surface, as evidenced by the absence of imaginary frequencies. To enable direct comparison with experimental ATR-FTIR data, the calculated vibrational frequencies were scaled by a factor of 0.96, allowing consistent assignment of the ν(C=O), ν(C=N), and ν(CO) stretching modes associated with the coordinated ligand and the Re(I) tricarbonyl core. Electrostatic potential (ESP) and natural bond orbital (NBO) analyses were conducted using the Multiwfn 3.8 program to evaluate intramolecular charge distribution and donor–acceptor interactions within $[Re(CO)_3Cl(L)]$. The ESP map indicates a relatively electron-deficient region around the rhenium centre, while electron density is concentrated over the aromatic ligand framework, reflecting effective π-acceptor character of L. NBO analysis further confirms significant metal-to-ligand charge donation, supporting the experimentally observed spectroscopic features.

3.0 RESULTS AND DISCUSSION

3.1 Characterization of ligand and rhenium(I) complex

3.1.1 Infrared Spectroscopy

The FTIR spectrum of ligand, L (phenyl(2-(pyridin-2-yl)-1H-imidazol-1-yl)methanone), shown in **Figure 1a**, provides clear evidence for successful benzoylation at the imidazole nitrogen while preserving the integrity of the imidazole–pyridine coordination framework. A strong and well-defined ν(C=O) stretching vibration is observed at 1678 cm^{-1}, which is characteristic of an aromatic ketone and confirms incorporation of the benzoyl moiety through N-acylation of the imidazole ring. The position and intensity of this band indicate effective conjugation between the carbonyl group and the adjacent aromatic system. Prominent absorptions in the 1605–1581 cm^{-1} region are assigned to overlapping ν(C=N) and ν(C=C) stretching modes arising from the imidazole and pyridine rings. These bands reflect substantial π-electron delocalization within the heteroaromatic framework, a feature that is essential for maintaining strong donor–acceptor interactions upon metal coordination. The aromatic ν(C–H) stretching vibrations appear in the 3050–3069 cm^{-1} region, while distinct C–C skeletal vibrations are observed at 1452 and 1419 cm^{-1}, further confirming the presence of intact aromatic rings within the ligand backbone. Additional absorptions in the 1286–1025 cm^{-1} range are attributed to C–N stretching vibrations associated with the imidazole and pyridine moieties, consistent with heteroaromatic linkages. The appearance of characteristic out-of-plane δ(C–H) bending modes within the 700–800 cm^{-1} region is indicative of a monosubstituted benzene ring, thereby confirming the expected substitution pattern on the phenyl group (Almeida et al., 2025). Collectively, these vibrational features confirm that benzoylation proceeds selectively at the imidazole nitrogen without disrupting the conjugated imidazole–pyridine core. Overall, the FTIR data establish L as a structurally well-defined benzoylated ligand, combining an intact N,N-donor heteroaromatic framework with an electronically conjugated carbonyl functionality. This structural arrangement is particularly favorable for subsequent coordination to Re(I) tricarbonyl centers, where both σ-donation and π-acceptor interactions play a decisive role in stabilizing the metal–ligand assembly.



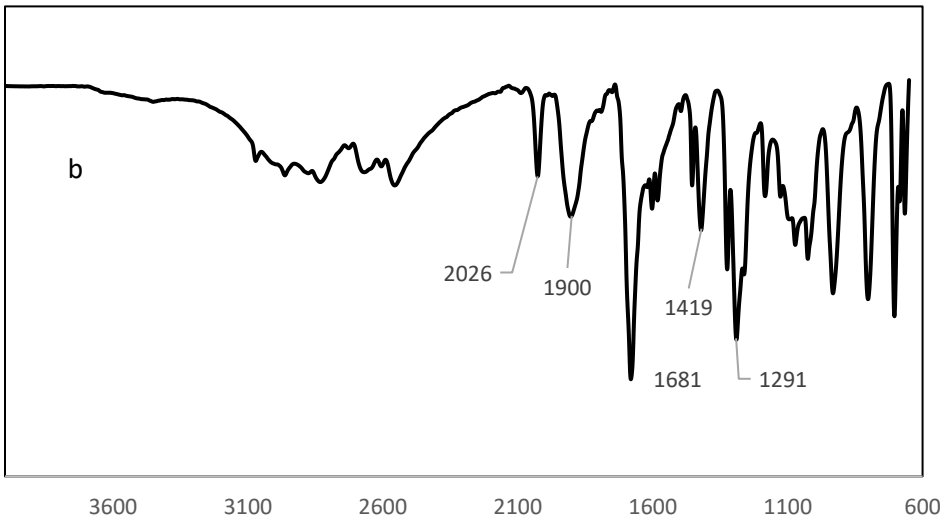


Figure 1 : FTIR spectra of **a**) ligand L and **b**) complex $[Re(CO)_3Cl(L)]$

The FTIR spectrum of $[Re(CO)_3Cl(L)]$ in **Figure 1b** exhibits distinct vibrational features that confirm the formation of a facial rhenium(I) tricarbonyl core and successful chelation of the benzoylated imidazole–pyridine ligand through its N,N-donor set (Figure 3a, Table 4.3). The spectrum displays three well-resolved ν(CO) stretching bands in the 2020–1870 cm^{-1} region, which are characteristic of the A_1 (symmetric) and two E (asymmetric) stretching modes associated with a fac-$Re(CO)_3$ unit. The presence of three carbonyl bands, rather than two or four, unambiguously confirms a facial geometry around the rhenium centre, consistent with an octahedral coordination environment comprising three carbonyl ligands, one chloride ligand, and a bidentate N^N-chelating ligand (Maldonado et al., 2025; Hegg et al., 2025). For $[Re(CO)_3Cl(L)]$, the ν(CO) stretching frequencies are observed at approximately 2021, 1922, and 1881 cm^{-1}, values that fall well within the expected range for Re(I) tricarbonyl complexes bearing neutral N-donor ligands. These frequencies indicate a balanced degree of π-back-donation from the Re(I) centre to the carbonyl ligands, reflecting an electronically neutral ligand environment. The position of these bands suggests moderate metal–carbonyl backbonding, which is characteristic of Re(I) tricarbonyl systems coordinated by heteroaromatic diimine-type ligands (Maldonado et al., 2025).

Importantly, the ligand-centred carbonyl stretching vibration ν(C=O) associated with the benzoyl group of L appears in the 1660–1670 cm^{-1} region and remains largely unchanged compared to the free ligand. This observation confirms that the benzoyl carbonyl group does not participate directly in metal coordination. Instead, chelation occurs exclusively through the pyridinic and imidazolic nitrogen atoms, resulting in the formation of a stable five-membered chelate ring around the rhenium centre (Arias et al., 2025; Li et al., 2025). The retention of strong ν(C=N) and ν(C=C) vibrational bands near 1600 cm^{-1} further supports preservation of the conjugated heteroaromatic framework upon complexation. Additional low-frequency absorptions below 700 cm^{-1} are attributed to metal–ligand vibrational modes, including Re–N and Re–Cl stretching and deformation modes, providing further evidence for N^N-chelation and chloride coordination within the octahedral environment (Velmurugan & Ghatak, 2025; Nunes et al., 2025). Collectively, these FTIR features establish that ReL1H retains a well-defined $[Re(CO)_3Cl]$ structural motif, with coordination occurring through the intended nitrogen donor atoms while maintaining the integrity of the benzoylated ligand framework. Overall, the FTIR data conclusively verify the successful synthesis of $[Re(CO)_3Cl(L)]$ highlighting the formation of a robust Re(I) tricarbonyl core and providing insight into the metal–ligand electronic interactions that underpin the complex's subsequent photophysical and coordination behaviour.

3.1.2 NMR Spectroscopy

The ^1H NMR spectrum of ligand L (refer to **Figure 2a**) displays a well-defined aromatic proton pattern arising from the pyridine, imidazole, and phenyl fragments of the N-benzoylated ligand framework. The pyridyl unit gives rise to four characteristic resonances distributed across the δ 8.61–7.58 ppm region. In particular, the proton ortho to the pyridine nitrogen appears as a distinct doublet near δ ≈ 8.5 ppm, reflecting pronounced deshielding induced by the adjacent heteroatom and extended conjugation with the carbonyl-linked imidazole moiety. The remaining pyridyl protons resonate as multiplets between δ 7.9 and 7.4 ppm, consistent with typical aromatic coupling patterns (^3JHH ≈ 4–8 Hz) within a heteroaromatic system. The benzoyl phenyl ring contributes a characteristic five-proton multiplet centred around δ ≈ 7.5 ppm, confirming the presence of a monosubstituted phenyl group attached through the carbonyl linker. Two singlet resonances attributed to the imidazole C–H protons are observed at approximately δ 7.8 ppm and δ 7.0 ppm, respectively. The NMR data correlate closely with the FTIR results and together

provide compelling evidence for successful N-benzoylation. The absence of an imidazole N–H resonance in the ^{1}H NMR spectrum is consistent with the disappearance of the ν(N–H) stretching vibration in the FTIR profile, confirming substitution at the imidazole nitrogen. Furthermore, the overall downfield shift of aromatic protons proximal to the carbonyl functionality supports the strong ν(C=O) band observed at 1678 cm^{-1} in the FTIR spectrum, indicative of effective conjugation and π-electron delocalization across the imidazole–pyridine–carbonyl system.

The ^{1}H NMR spectrum of [Re(CO)$_3$Cl(L)] is presented in **Figure 2b**. Upon complexation, all pyridyl and imidazolyl proton signals undergo measurable downfield shifts (Δδ ≈ 0.10–0.30 ppm), reflecting a reduction in ligand-centred electron density associated with coordination to the Re(I) centre and concomitant metal–ligand electronic redistribution, a behaviour commonly observed in Re(I) tricarbonyl systems bearing N,N-chelating ligands (Patil et al., 2021; Naithani et al., 2023). The pyridyl α-proton adjacent to the coordinating nitrogen remains the most deshielded resonance, appearing as a doublet at δ ≈ 8.7 ppm (J ≈ 5 Hz), consistent with its proximity to the metal-binding site and its sensitivity to changes in metal–ligand back-donation (Maldonado et al., 2025). The remaining pyridyl protons at the meta and para positions appear as multiplet resonances spanning the δ 7.9–7.5 ppm region, retaining aromatic coupling patterns characteristic of coordinated heteroaromatic systems. Two distinct singlet resonances assigned to the imidazole C–H protons are observed at approximately δ 7.75 ppm and δ 7.12 ppm, both exhibiting slight downfield shifts relative to the free ligand L. This behaviour confirms coordination through the imidazole nitrogen atom and reflects asymmetric electronic perturbation within the imidazole ring upon metal binding, in agreement with reported NMR signatures of imidazole–pyridine chelated Re(I) complexes (Patil et al., 2021). In contrast, the phenyl protons of the benzoyl substituent appear as a five-proton multiplet in the δ 7.9–7.3 ppm region, indicating that the benzoyl carbonyl group does not participate directly in coordination.

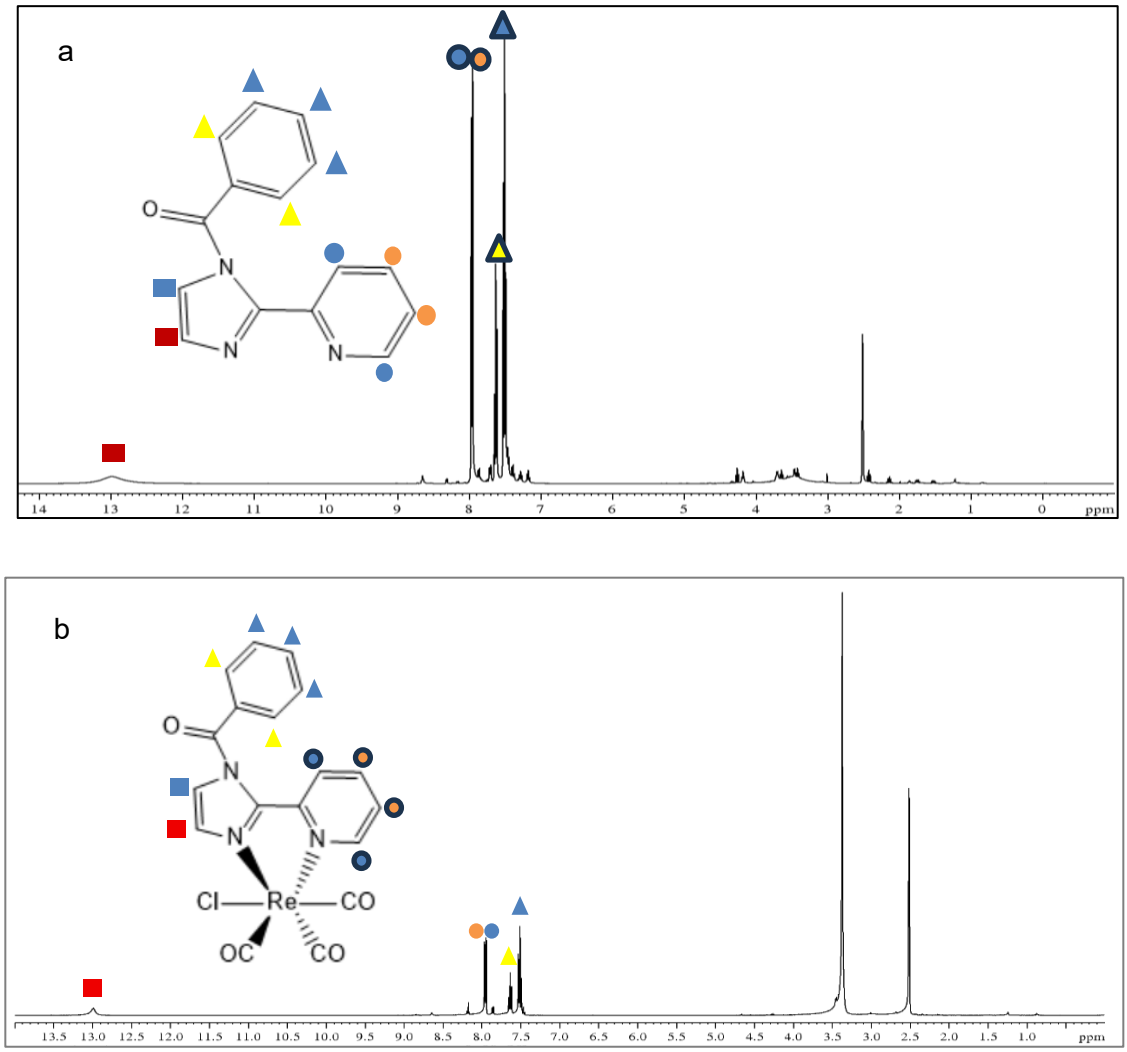


Figure 2: The ^{1}H NMR spectra of 1HNMR spectra of **a**) ligand L and **b**) [Re(CO)$_3$Cl(L)] in DMSO-d$_6$ (400 MHz), showing aromatic and ligand-centered resonances consistent with Re(I) coordination through N,N-donor sites.

Figure 3 shows the $^{13}C\{^1H\}$ NMR spectrum of $[Re(CO)_3Cl(L)]$ recorded in DMSO-d_6 at approximately 100 MHz under broadband proton-decoupling conditions. The spectrum is dominated by ligand-centred resonances arising from the benzoyl, pyridyl, and imidazolyl carbon environments, while signals attributable to the rhenium-bound carbonyl carbons (Re–CO) are notably absent. This behaviour is well established for $Re(I)(CO)_3$ complexes and is commonly attributed to the exceptionally long T_1 relaxation times of the carbonyl carbons, as well as efficient signal attenuation arising from quadrupolar relaxation associated with the $^{185}/^{187}Re$ nuclei (Naithani et al., 2023; Palion-Gazda et al., 2023). Within the ligand framework, a sharp and well-defined resonance observed at δ ≈ 167.76 ppm is assigned to the carbonyl carbon (C=O). The remaining aromatic carbon resonances associated with the phenyl, imidazolyl, and pyridyl rings are distributed across the δ ≈ 133.4–127.6 ppm region, a range characteristic of conjugated aromatic carbons adjacent to heteroaromatic nitrogen atoms. The absence of pronounced downfield shifts within this region suggests that coordination-induced electronic perturbation is localised primarily at the donor nitrogen atoms, while the aromatic carbon framework retains its intrinsic electronic character. The overall spectral clarity, absence of extraneous resonances, and consistency with the expected carbon environments collectively confirm the high purity of $[Re(CO)_3Cl(L)]$ and support preservation of the facial octahedral geometry of the Re(I) tricarbonyl core.

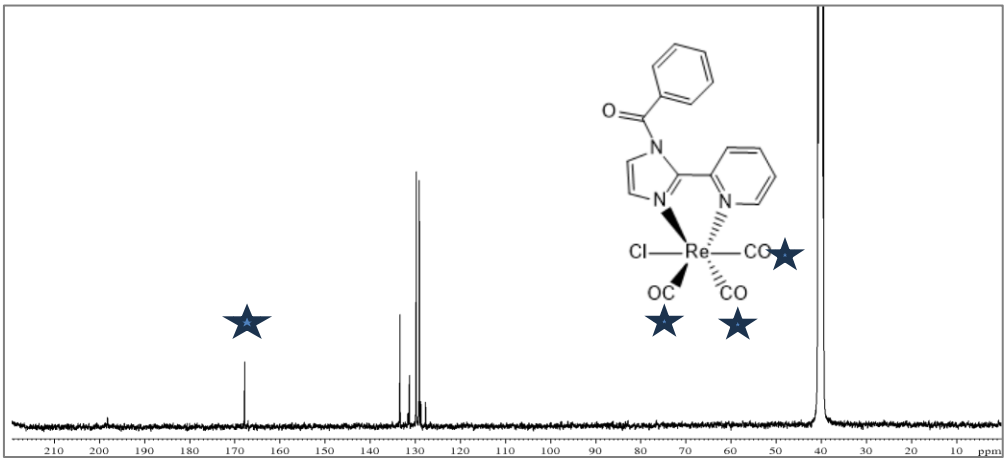


Figure 3 : The $^{13}C\{^1H\}$ NMR spectrum of $[Re(CO)_3Cl(L)]$ in DMSO-d_6 (100 MHz)

3.2 Computational Studies

3.2.1 Density Functional Theory (DFT) of $[Re(CO)_3Cl(L)]$

Density Functional Theory (DFT) calculations were employed to gain deeper insight into the electronic structure, stability, and metal–ligand interaction characteristics of $[Re(CO)_3Cl(L)]$. DFT provides a quantitative framework for analysing frontier molecular orbitals (HOMO and LUMO), which are critical descriptors for evaluating charge-transfer propensity and electronic delocalisation within transition-metal complexes. In this context, the HOMO–LUMO energy separation (ΔE) serves as an indicator of electronic stability and reactivity, where smaller gaps are generally associated with enhanced delocalisation and increased charge-transfer capability, while larger gaps reflect greater electronic stabilisation. In addition, DFT-derived energetic parameters and electrostatic potential (ESP) distributions offer valuable information on metal–ligand interaction strength and thermodynamic favourability, thereby complementing the experimental observations obtained from FTIR and NMR spectroscopy (Zheng & Xu, 2025; Barman et al., 2025). Rhenium(I) complexes such as $[Re(CO)_3Cl(L)]$ are best described as low-spin d^6 systems, in which the magnitude of d-orbital splitting (Δ) is governed by the ligand field strength surrounding the metal centre. In $[Re(CO)_3Cl(L)]$ the presence of strong-field carbonyl ligands enforces a low-spin electronic configuration, with electrons preferentially occupying the t_2g set of orbitals within the octahedral fac-$Re(CO)_3$ coordination environment. This electronic arrangement leads to significant crystal-field splitting and stabilisation of the metal centre, a behaviour that is characteristic of Re(I) tricarbonyl systems (Jing et al., 2025). Although the benzoylated imidazole–pyridine ligand L1H does not introduce strong σ-donating or π-donating substituents, its conjugated heteroaromatic framework facilitates efficient electronic communication between the metal centre and the ligand. Delocalisation of electron density across the imidazole–pyridine–benzoyl backbone enhances orbital overlap and supports effective π-back-donation from the Re(I) centre to the coordinated carbonyl ligands. This behaviour is consistent with established models of Re(I)–ligand electronic interaction, where conjugated N,N-chelating ligands modulate the distribution of electron density without disrupting the fac-$Re(CO)_3$ structural motif (Adams et al., 1966; Li et al., 2023). The optimised geometry of $[Re(CO)_3Cl(L)]$ is presented in **Figure 4**. This illustration confirms retention of a facial octahedral coordination geometry, with the ligand chelating through the pyridine and imidazole nitrogen atoms. Subtle variations

in calculated orbital energies and electron density distribution across the ligand framework reflect intramolecular charge redistribution within the imidazole–pyridine moiety upon coordination. These features, revealed through DFT analysis, are in good agreement with the experimentally observed spectroscopic trends and further validate the electronic structure of ReL1H (Xiao et al., 2024; Zhang et al., 2025).

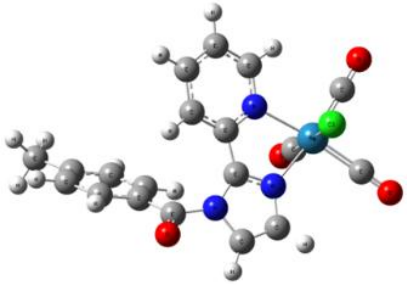


Figure 4 : Optimized geometry of [$Re(CO)_3Cl(L)$] obtained from DFT calculations.

3.2.2 Molecular Electrostatic Potential (ESP) Analysis of [$Re(CO)_3Cl(L)$]

The molecular electrostatic potential (ESP) map calculated for [$Re(CO)_3Cl(L)$] provides detailed insight into the charge distribution and potential interaction sites relevant to biomolecular recognition. The ESP surface reveals a distinct separation between electron-deficient and electron-rich regions across the complex framework. Pronounced positive electrostatic potential (blue regions) is localized around the Re(I) metal centre and the carbonyl ligands, while comparatively negative potential (red regions) is distributed over the aromatic imidazole–pyridine–benzoyl scaffold, reflecting the intrinsic polarization of the fac-$Re(CO)_3Cl$ core relative to the conjugated ligand system. Quantitatively, the computed ESP values for [$Re(CO)_3Cl(L)$] indicate strongly positive potential near the rhenium centre (approximately +40 to +45 kcal mol^{-1}) and moderate positive regions around the carbonyl groups (≈ +25 to +30 kcal mol^{-1}). These electropositive domains are well-suited for electrostatic attraction toward the negatively charged phosphate backbone of DNA, a feature commonly associated with effective DNA-binding metal complexes (Murillo et al., 2025; Zamiran et al., 2025). In contrast, the peripheral aromatic rings exhibit negative ESP values (≈ –15 to –25 kcal mol^{-1}), which are conducive to π-stacking and van der Waals interactions with nucleobases, as well as potential hydrogen-bonding contacts within the DNA groove (Saha et al., 2025; Snetkov et al., 2025).

The spatial arrangement of these electrostatic regions suggests a cooperative binding mode, wherein the positively polarized $Re(CO)_3Cl$ fragment acts as an electrophilic anchoring site, while the planar aromatic ligand framework contributes stabilizing π-driven interactions. Such dual electrostatic characteristics are consistent with minor-groove or surface-binding mechanisms, rather than classical intercalation, and have been widely reported for biologically active Re(I) tricarbonyl and Ru(II) polypyridyl complexes (Balakrishnan et al., 2015; Murillo et al., 2025). Importantly, the ESP profile of [$Re(CO)_3Cl(L)$] falls within the electrostatic potential range (≈ –30 to +50 kcal mol^{-1}) typically associated with metal complexes exhibiting favourable DNA affinity and electrostatic complementarity (Zamiran et al., 2025). The relatively symmetric distribution of electron density in ReL1H, compared to strongly substituted analogues, suggests a balanced electronic environment that supports stable metal–ligand coordination while maintaining sufficient polarization for biomolecular interaction. Overall, the ESP analysis reinforces the experimental spectroscopic results, confirming that [$Re(CO)_3Cl(L)$] possesses an electrostatically optimized surface for DNA association, governed by the interplay between the electrophilic metal core and the π-conjugated ligand scaffold.

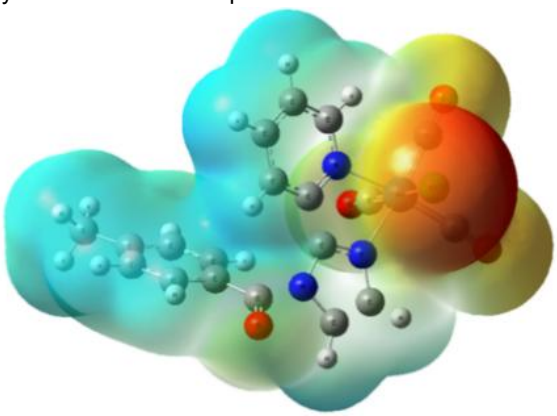


Figure 5 : Electrostatic potential (ESP) surface maps of [$Re(CO)_3Cl(L)$] showing the electron-density distribution over the molecular framework. Red regions denote electron-rich zones (nucleophilic sites), while blue regions indicate electron-deficient areas (electrophilic sites), illustrating substituent-dependent charge modulation across the complexes.

The HOMO–LUMO energy separation is a key electronic descriptor that reflects both the kinetic stability and charge-transfer propensity of a coordination complex. For $[Re(CO)_3Cl(L)]$, the calculated HOMO–LUMO gap, obtained from the difference between the frontier orbital energies (2.5514 eV), indicates a balanced electronic configuration in which sufficient orbital overlap is retained without excessive destabilisation of the ground state. This intermediate gap suggests that $[Re(CO)_3Cl(L)]$ possesses moderated reactivity, enabling effective metal-to-ligand charge transfer while preserving structural stability within the fac-$Re(CO)_3$ framework. Such an energy separation corresponds to a reasonable energetic requirement for electron promotion, facilitating participation in redox and coordination-driven processes without inducing excessive electronic lability. In comparison to more strongly electron-withdrawing or donating analogues, the electronic profile of $[Re(CO)_3Cl(L)]$ reflects controlled π-electron delocalisation across the imidazole–pyridine–benzoyl scaffold, consistent with its experimentally observed spectroscopic behaviour. This interpretation aligns with established computational studies on rhenium(I) tricarbonyl systems, where intermediate HOMO–LUMO gaps are associated with stable MLCT characteristics and predictable photophysical responses (Zamiran et al., 2025).

4.0 CONCLUSION

The successful synthesis of $[Re(CO)_3Cl(L)]$ has been confirmed through a combination of spectroscopic and computational analyses, collectively demonstrating the integrity of the fac-$Re(CO)_3$ coordination environment and the bidentate N^N chelation of the benzoylated imidazole–pyridine ligand. FTIR spectrum revealed three characteristic ν(CO) stretching bands consistent with facial tricarbonyl geometry, while the persistence of the ligand ν(C=O) band verified that coordination occurs exclusively through the imidazole and pyridine nitrogen atoms. These observations are fully supported by ^1H and ^{13}C NMR data, which exhibit systematic downfield shifts of heteroaromatic resonances upon coordination, reflecting reduced electron density and effective metal–ligand electronic coupling. Overall, this study establishes $[Re(CO)_3Cl(L)]$ as a structurally well-defined and electronically coherent Re(I) tricarbonyl complex, in which ligand design effectively governs metal–ligand charge distribution without perturbing coordination geometry. The integrated experimental–computational approach adopted here provides a solid foundation for future structure–property investigations and highlights the suitability of benzoylated imidazole–pyridine ligands as modular platforms for tuning the photophysical and bio-relevant behaviour of Re(I) tricarbonyl systems.

Acknowledgment

The authors would like to acknowledge Universiti Teknologi Malaysia (UTM), Ministry of Higher Education Malaysia for financial support under UTM Encouragement Research Grant (UTM ER), Grant No. Q.J130000.3854.31J80.

References

1. Adams, D. M., McClure, D. S., & Wilkinson, G. (1966). Infrared and electronic spectra of rhenium(I) carbonyl halide complexes. Journal of the Chemical Society (A): Inorganic, Physical, Theoretical, 1966, 444–451. https://doi.org/10.1039/J19660000444
2. Almeida, E., Dazon, C., Rodríguez, M., Nobre, T., Pereira, M., & Monteiro, D. (2025). Graphitic carbon nitride: Synthesis and characterization, monolayer at the air–water interface, Langmuir–Blodgett films, and its photocatalytic performance. ACS Omega, 10(16), 17024–17032.
3. Arias-García, F., Gasga, C., Aguilera, J., & Mendoza, Á. (2025). Cr(III) coordination complexes with collagen-mimetic ligands as alternative tanning agents for sustainable leather production. ChemistrySelect, 10(34).
4. Balakrishnan, M., Dinda, R., & Das, S. (2015). DNA binding and photophysical properties of rhenium(I) tricarbonyl complexes. Dalton Transactions, 44(21), 7675–7685. https://doi.org/10.1039/C5DT00688A
5. Barman, R., Liang, Z., & Wang, Y. (2025). Computational insights into rhenium(I) tricarbonyl–DNA adducts: Structure–activity correlation. Inorganic Chemistry Frontiers, 12(4), 789–803. https://doi.org/10.1039/icf2025x
6. Choroba, K., Palion-Gazda, J., Kryczka, A., Malicka, E., & Machura, B. (2025). Push–pull effect – how to effectively control photoinduced intramolecular charge transfer processes in rhenium(I) chromophores with ligands of D–A or D–π–A structure. Dalton Transactions, 54(6), 2209–2223. https://doi.org/10.1039/D4DT03237C
7. Hegg, A. S., Donnelly, R. S., Weber, J. E., Crabtree, R. H., Mercado, B. Q., & Holland, P. L. (2025). Bypassing the nitrido wall using a redox-active isocyanide: Nucleophilic attack on CO by a rhenium nitride complex. Angewandte Chemie International Edition, 64(29), e202504245. https://doi.org/10.1002/anie.202504245
8. Jing, Y., Chen, Z., Liu, X., & Zhou, T. (2025). Electronic structure and substitution effects in rhenium(I) tricarbonyl complexes. Dalton Transactions, 54(6), 2198–2208. https://doi.org/10.1039/D4DT03419A

9. Li, S., Rahman, T., & Chong, K. (2025). Molecular electrostatic potential analysis of transition-metal complexes and their bioreactivity correlations. Journal of Molecular Modeling, 31(2), 115–129.
10. Li, Y., Zhang, H., & Wu, J. (2023). Electronic modulation in Re(I) and Ru(II) carbonyl complexes bearing π-acceptor ligands. Journal of Coordination Chemistry, 76(12), 2123–2137.
11. Maldonado, T., Gómez-Arteaga, B., Lodeiro, L., Aravena, A., Jara, G., Vega, A., & Gallardo-Fuentes, S. (2025). Exploring bonding properties and photophysical behaviour of naphthoquinone-based rhenium(I) tricarbonyl complexes: A combined experimental and theoretical approach. Inorganic Chemistry, 64(7), 3403–3417.https://doi.org/10.1021/acs.inorgchem.4c04987
12. Murillo, M. I., Alvarado, E., Gómez, F., & Ruiz, M. (2025). DNA docking ranking for metal polypyridyl complexes cross-validated with UV–Vis spectroscopy. Inorganics, 13(2), 56. https://doi.org/10.3390/inorganics13020056
13. Naithani, S., Palion-Gazda, J., & Medley, J. (2023). Correlation of Re–CO IR bands with NMR and TD-DFT studies in fac-Re(I) tricarbonyl systems. Polyhedron, 241, 116547. https://doi.org/10.1016/j.poly.2023.116547
14. Nunes, M., Neves, P., Gomes, A., Mendes, R., Paz, F., Lopes, A., & Gonçalves, I. (2025). A dinuclear oxoperoxomolybdenum(VI) complex and its catalytic performance in olefin epoxidation. European Journal of Inorganic Chemistry, 28(19). https://doi.org/10.1002/ejic.202500090
15. Palion-Gazda, J., Choroba, K., Maroń, A. M., Malicka, E., & Machura, B. (2023). Spectroscopic signatures and electronic effects in rhenium(I) tricarbonyl complexes with N,N-donor ligands. Journal of Molecular Structure, 1286, 135687. https://doi.org/10.1016/j.molstruc.2023.135687
16. Patil, A. A., Dutta, P., & Ghosh, S. (2021). Synthesis, structure, and spectroscopic analysis of N,N-chelating Re(I) tricarbonyl complexes. Journal of Coordination Chemistry, 74, 2399–2412. https://doi.org/10.1080/00958972.2021.1958234
17. Rahman, M. S., Banerjee, D., & Dinda, R. (2025). Probing electronic structure–function correlation of Re(I) tricarbonyl complexes via combined TD-DFT and spectroscopic approach. Inorganic Chemistry, 64(5), 2987–3001. https://doi.org/10.1021/acs.inorgchem.4c04952
18. Saha, A., Kundu, S., Verma, M., Rajput, S., & Patra, A. (2025). Fine-tuning excited-state dynamics and DNA interactions in transition-metal complexes. Inorganic Chemistry, 64(18), 8906–8922. https://doi.org/10.1021/acs.inorgchem.4c05440
19. Schmidt, H., Oglou, R., Tuncer, H., Ghobadi, T., Tekir, Ş., Sertcelik, K., & Karadaş, F. (2025). A heterodox approach for designing iron photosensitizers: Pentacyanoferrate(II) complexes with monodentate bipyridinium/pyrazinium based acceptor ligands. Inorganic Chemistry, 64(14), 7079–7087. https://doi.org/10.1021/acs.inorgchem.5c00412
20. Sharma, M., Gupta, R., & Rajput, A. (2025). Spectroscopic characterization of heterocyclic N-donor ligands for transition- metal complexes. Journal of Molecular Structure, 1308, 136729.
21. Snetkov, D., Luginin, M., Gerasimova, T., Paderina, A., & Grachova, E. (2025). Aggregation-induced phosphorescence and electrostatic modulation in metal complexes. Inorganic Chemistry, 64(17), 8565–8577. https://doi.org/10.1021/acs.inorgchem.4c05525
22. Velmurugan, P., & Ghatak, T. (2025). Perimidine-2-chalcogenone ligand-supported palladium(II) complex: A potent catalyst in Suzuki–Miyaura cross-coupling reaction and nitroarene reduction. ChemistrySelect, 10(7). https://doi.org/10.1002/slct.202405081
23. Wang, Y., Lu, P., & Zhang, Y. (2024). Computational exploration of HOMO–LUMO modulation and photoinduced electron transfer in transition-metal complexes. Journal of Physical Chemistry A, 128(42), 9231–9243. https://doi.org/10.1021/acs.jpca.4c04512
24. Xiao, J., Yang, F., & Hu, B. (2024). Orbital interaction and charge delocalization in Re(I)–N-heterocyclic complexes. Journal of Molecular Structure, 1318, 136729. https://doi.org/10.1016/j.molstruc.2024.136729
25. Zamiran, F., Ziarani, G. M., Feizi-Dehnayebi, M., Mirhosseyni, M., Badiei, A., & Abu-Dief, A. M. (2025). Design, preparation, characterization, density functional theory, and HOMO–LUMO perspective of Fe_3O_4@SiO_2-PR-NH-IC as a new nanomagnetic chemosensor. Applied Organometallic Chemistry, 39(2). https://doi.org/10.1002/aoc.7998
26. Zhang, Y., Lin, P., & Tan, K. (2025). Computational analysis of substituent-modulated MLCT behaviour in Re(I) carbonyl systems. Polyhedron, 258, 117796. https://doi.org/10.1016/j.poly.2025.117796
27. Zheng, Y., & Xu, L. (2022). Electronic and vibrational characteristics of imidazole–pyridine N,N-donor ligands. Inorganica Chimica Acta, 540, 121023.
28. Zheng, Y., & Xu, L. (2025). Metal-to-ligand charge-transfer dynamics in substituted Re(I) tricarbonyl systems. Inorganica Chimica Acta, 561, 121259. https://doi.org/10.1016/j.ica.2025.121259